END
DATE
FILMED
7 84
DTIC

MICROCOPY RESOLUTION TEST CHART

NATIONAL BUREAU OF STANDARDS 1963 A

OFFICE OF NAVAL RESEARCH

Determination of Structural Parameters from EXAFS:

Application to Solutions and Catalysts

by

Donald R. Sandstrom

Washington State University
Department of Physics
Pullman, WA 99164-2814

DTIC
ELECT
JUN 1 9 1984
S

May 23, 1984

84 06 18 066

REPORT DOCUMENTATION PAGE		READ INSTRUCTIONS BEFORE COMPLETING FORM
1. REPORT NUMBER Technical Report No. 3	2. GOVT ACCESSION NO. AD-A142205	3. RECIPIENT'S CATALOG NUMBER
4. TITLE *(and Subtitle)* Determination of Structural Parameters from EXAFS: Application to Solutions and Catalysts		5. TYPE OF REPORT & PERIOD COVERED Technical Report
		6. PERFORMING ORG. REPORT NUMBER
7. AUTHOR(s) Donald R. Sandstrom		8. CONTRACT OR GRANT NUMBER(s) N00016-82-K-0530
9. PERFORMING ORGANIZATION NAME AND ADDRESS Department of Physics Washington State University Pullman, WA 99164-2814		10. PROGRAM ELEMENT, PROJECT, TASK AREA & WORK UNIT NUMBERS
11. CONTROLLING OFFICE NAME AND ADDRESS Leader, Chemistry Division Office of Naval Research 800 North Quincy Street Arlington, Virginia 22217		12. REPORT DATE May 23, 1984
		13. NUMBER OF PAGES 43
14. MONITORING AGENCY NAME & ADDRESS*(if different from Controlling Office)* Office of Naval Research Resident Representative, University of Washington District Building, Room 422 1107 Northeast 45th St. Seattle, Washington 98195		15. SECURITY CLASS. *(of this report)* Unclassified
		15a. DECLASSIFICATION/DOWNGRADING SCHEDULE

16. DISTRIBUTION STATEMENT *(of this Report)*

This document has been approved for public release and sale; its distribution is unlimited.

17. DISTRIBUTION STATEMENT *(of the abstract entered in Block 20, if different from Report)*

18. SUPPLEMENTARY NOTES

19. KEY WORDS *(Continue on reverse side if necessary and identify by block number)*

EXAFS, solutions, catalysts, analysis procedures

20. ABSTRACT *(Continue on reverse side if necessary and identify by block number)*

A review is presented of applications of Extended X-Ray Absorption Fine Structure (EXAFS) spectroscopy to the determination of structural detail in inorganic solutions and supported metal catalyst particles. Similarities in these applications are noted and the possible role of disorder on the reliability of the EXAFS results is discussed. A brief summary of data analysis procedures is presented with examples.

DD FORM 1473
1 JAN 73

Determination of structural parameters from EXAFS: Application

to solutions and catalysts

Donald R. Sandstrom

Department of Physics, Washington State University, Pullman,

Washington 99164, USA

Abstract

A review is presented of applications of Extended X-Ray

Absorption Fine Structure (EXAFS) spectroscopy to the determina-

tion of structural detail in inorganic solutions and supported

metal catalyst particles. Similarities in these applications

are noted and the possible role of disorder on the reliability

of the EXAFS results is discussed. A brief summary of data

analysis procedures is presented with examples.

INTRODUCTION

The scope of the present paper is to review briefly the application of EXAFS spectroscopy to the study of local order and structure in inorganic solutions, and to the study of supported metal catalysts. These areas, while weakly related in terms of application, have common factors relative to their examination by EXAFS. These include a comparatively large degree of disorder, coordination of metal atoms both by low-Z scattering atoms such as O and C and higher-Z atoms such as Br and Pt, and by the need to measure the x-ray absorption spectrum for the metal atoms at low concentration in a low-Z matrix.

In addition to the above review, an overview will be given of the analysis procedures appropriate for these systems. This will include the steps involved in the extraction of the EXAFS oscillations from the raw experimental data, as well as analysis of the EXAFS spectrum for structural detail. Particular attention will be given to evaluation of the phase information present in the EXAFS spectrum, and handling of the k-dependent phase functions, especially for high-Z scatterers such as Pt.

APPLICATIONS TO SOLUTIONS

The past few years have seen very significant advances in our understanding of structure present in aqueous solutions. These have come partly as a result of theoretical studies[1] and partly as a result of the application of experimental techniques of which EXAFS is one. The experimental methods give direct evidence for the existence of a first hydration zone such as described by Frank and Wen,[2] with evidence for a second zone in many cases.

Historically, the experimental study of solutions employed optical and resonance spectroscopy and thermodynamic measurements. Since the 1960's these have been supplemented by x-ray and neutron diffraction methods.[3] The diffraction techniques have been strongly developed during the past decade, and now represent the principal methods in use. Although EXAFS spectroscopy was applied to a solution system as early as 1975,[4] most contributions to our understanding of solutions from this source have come since 1978.

Because of the important role which x-ray and neutron diffraction play in current research, the contributions of EXAFS spectroscopy can best be discussed in the context of these two techniques. A comprehensive review of diffraction methods has recently been given by Neilson and Enderby.[3] Both techniques measure the differential scattering cross section $d\sigma/d\Omega$ as a function of the scattering vector or momentum transfer $k = (4\pi/\lambda)\sin(\Theta/2)$, where the full range of k from very small values out to ~15 Å^{-1} can be measured. Because the momentum transfer in the electron scattering involved in EXAFS is twice the conventionally displayed electron wave vector k, the above range of momentum transfer for the diffraction case can be compared to a momentum transfer range of $6 < 2k < 3.0 \text{ Å}^{-1}$ for the typical EXAFS case. Loss of the low k data in the EXAFS case has been pointed out[5] to be responsible for reduced ability to recover slowly varying portions of the radial distribution

functions from Fourier transforms of the EXAFS spectra, in contrast to the diffraction case.

Measured diffraction curves derive from a total structure factor that is a linear superposition of terms involving partial structure factors for each distinct atom-atom correlation present in the system. For example, a four component system such as MX_n dissolved in H_2O would involve ten partial structure factors. The challenge of unraveling details of the pertinent M-O, M-X or X-O coordinations from the data has been met with considerable success by modeling procedures, and in the case of neutron diffraction, by isotopic sub-stitution methods.[3] It should be noted that the availability of tunable syn-chrotron radiation offers the possibility of using the anamolous dispersion of the elements in the solution to attack this problem.[6] With EXAFS, one measures a superposition of the coordinations involving each accessible element in turn because of the spectroscopic separation of the absorption edges of the elements. The resulting element specificity is a key advantage in that the modeling of the EXAFS spectra is very much simplified compared to the diffraction case, especially when no structural evidence is available in advance.

Diffraction techniques become increasingly difficult to apply when concentration is below the range 0.1 - 1.0 M, because of the then overwhelming effect of the solvent-solvent correlations. At lower concentrations, EXAFS has considerable advantage, as fluorescence detection techniques can extend detectability to 100 ppm or below.[7]

The first applications of EXAFS spectroscopy to solution studies emphasized hydrated ions at low concentrations in aqueous solutions. These included the work of Eisenberger and Kincaid[4] and Sandstrom et al.[8,9] The primary objective of each of these studies was the determination of bond lengths to water molecules in the first hydration spheres of the cations or anions. These results are summarized in Table I.

In the first study shown in Table I, bond length was estimated directly from the wavelength of the EXAFS oscillations in k-space by applying a correction factor for the k-dependent phase function obtained from a reference material. The second study proceeded similarly, but the correction was applied to the position of the peak in the Fourier transform of the EXAFS oscillations. In the work reported in Ref. 9, bond lengths were obtained by a phase fitting method that will be described in more detail below. Where applicable, close agreement was found between the bond lengths shown in Table I and results from x-ray diffraction studies.

Subsequent to the above studies, a major area of application of EXAFS spectroscopy has been to the concentrated I-II electrolytes. These systems have simultaneously received considerable attention from workers employing both x-ray and neutron diffraction, as well as Raman spectroscopy. Specifically, several workers have studied the concentrated chlorides and bromides of Ni, Cu, and Zn in aqueous solution. For these systems, the formation of complexes containing direct metal-halogen bonds as well as metal-water coordination has been postulated. In addition, evidence for longer range cation-cation ordering similar to that in the crystalline salt has been presented. A summary of recent evidence for these systems from all applicable techniques is presented in Table II.

The results for the NiCl solutions by the diffraction techniques and EXAFS appear at first sight to be in good agreement that the first coordination sphere of Ni^{2+} is fully hydrated. This statement must, however, be somewhat qualified because of real sensitivity limitations to minority species that exist for all of these techniques. As Magini points out,[11] in a 50% mixture of $Ni(H_2O)_6^{2+}$ and $NiCl(H_2O)_5^+$ the average Cl^- coordination of the Ni^{2+} ion is only 8.3%. When it is considered that such a minority correlation must be extracted,

in the case of the diffraction techniques, not only from the background of the $Ni-H_2O$ correlations but also from the other correlations present in the solution, it should not be surprising that uncertainty exists with respect to minority species. The situation is somewhat better with EXAFS because only ligands of the x-ray absorbing atom effect the spectrum, but distinguishing among low-Z coordinating atoms at, say, the 10% level is not easy even when amplitude and phase functions are accurately known. The situation is helped somewhat in the case of $NiCl_2$ by the fact that the Ni-O and Ni-Cl phase functions differ by about π over the entire k-range of interest.[14] It seems likely that the dis-agreement that stands between the diffraction-EXAFS results and the Raman results[16] is due partly to this weak sensitivity to minority species coupled with a high sensitivity of Raman to Ni-Cl bonds. Nevertheless, the diffraction and EXAFS results for $NiCl_2$ would not admit $NiCl_4^{2-}$ complexes at anything like the 50% level suggested by the Raman studies. Such a conclusion is supported by the one $NiBr_2$ study,[15] which confirms the picture of full hydration of Ni^{2+}. Much of the ambiguity concerning the possible Ni-Cl bonding is removed from this case because of the very much larger backscattering amplitude and different behavior of the phase function for a Br scatterer.

Studies of $CuCl_2$ (Table II) all show evidence for direct Cu-Cl bonding, but disagree on the degree of coordination and its significance in terms of the presence of any long-range structures in these solutions. At highest concen-trations, there does seem to be strong evidence for species, whether Cu monomers or polymers, having local coordination resembling that in the $CuCl_2$ crystal. This tendency appears to be enhanced when excess Cl^- ions are added to the solutions.[17]

Crystal-like local coordination seems to exist also in $CuBr_2$ at high concentrations. Here the question is the degree to which planer $CuBr_4^{2-}$ units

link up to form chains as in the crystal. For Cu^{2+} ions in such units, the Br coordination would be 4. Thus the reported[15,18] coordination number of 1.5 ± 0.5 would correspond to 25 - 50% of the Cu^{2+} ions in $CuBr_4^{2-}$ units if the remaining Cu^{2+} ions are completely hydrated. For the same solution, it is easy to show that the average number of Cu^{2+} ions coordinating each Br^- ion would be just twice the fraction of Cu^{2+} ions occupying $CuBr_4^{2-}$ units, independent of whether chains of any length are formed. This would correspond to 0.5 - 1.0 Cu^{2+} ion coordinating each Br^- ion on average, compared to 1.0 - 1.5 reported. This disagreement is not very significant, but could signal the presence of other Cu-Br containing species in these solutions besides $CuBr_4^{2-}$. Support for the idea of linked chains is given by the report of two unequal Br-Br bond distances in these solutions. The work of Fine[19] shows evidence for more than one species having slightly differing Cu-Br bond lengths. Variation of the Br/Cu ratio by adding HBr produced no change in these bond lengths, but strongly affected the relative abundance of the two species. The species have been tentatively identified as $CuBr(H_2O)^{5+}$ and $CuBr_4(H_2O)_2^{2-}$ with little evidence for chain formation of the latter. Whether real disagreement exists among the results for $CuBr_2$ solutions depends strongly on the confidence that can be attached to the absolute coordination numbers. Clearly the existing results need to be tested against various models for speciation, and improved measurements made.

Among the cations considered here, $ZnBr_2$ solutions show the most clear cut tendency to form long-range ordered structures. The linked $ZnBr_4$ tetrahedra reported persist in ethyl acetate[20] in which the dielectric constant is over an order of magnitude lower.

In all of the above discussion of the formation of ordered structures or complexes in solutions, it is clear that the ordering is dynamic in nature

to a lesser or greater degree. EXAFS and the diffraction techniques measure the time average of this dynamic structure, which means that all states of the evolution of the structure are factored in with weights proportional to the time spent in each state. If the lifetime of a particular configuration of atoms is long compared to the time it takes to form itself out of randomly associated atoms, then EXAFS or diffraction can give a fairly accurate picture of the structure because the average pair distribution function will reflect that of the quasi-stable configuration. If this pair distribution function is reasonably symmetric, then analysis of the data with the assumption of a Gaussian distribution will give accurate results.[5,21] This is the procedure that has been universally applied in solution EXAFS work to date. The determination of first sphere bond lengths is probably a good example of this situation, because of the generally good agreement between hydrated crystals and solutions, and among EXAFS and the diffraction techniques. On the other hand, an associated configuration having only very transitory existence, for which the coordinating atoms spend a large fraction of the time moving into and out of position, will exhibit a very asymmetric time average pair distribution function which does not reflect a bonding situation at all. Unless this is accurately taken into account, the EXAFS analysis will emphasize the distance of closest approach, and underestimate the bond lengths in the stable configuration, as discussed by Eisenberger and Brown.[5] Such an effect may be operating in the case of the second sphere Ni-Cl distance measured for $NiCl_2$ solutions of 3.1 Å,[14] because this bond length seems unreasonably short.[12]

Although the present discussion emphasizes the study of inorganic solutions by EXAFS spectroscopy, other important applications of EXAFS to solutions also exist. These include the large application area of biochemistry,[22] and homogeneous catalysis.[9,23,24]

APPLICATIONS TO CATALYSTS

The study of catalyst materials has formed one of the major application areas for EXAFS spectroscopy. Because this field is very large, and extensive reviews exist, only catalysis on solids,[25] or heterogeneous catalysis, and the contributions of EXAFS spectroscopy will be discussed here. These have also been reviewed recently, e.g. by Lytle et al.[26] and Lee et al.[27]

Supported metal catalysts[28] form the main area of application of EXAFS. Here a fortunate combination of circumstances makes EXAFS a probe ·y well suited to the application. For example, metal atom concentrations ε usually low, often below 1 wt. % in a low-Z matrix such as alumina, sili or a zeolite. The inherent sensitivity and spectroscopic element specificit, ∪f EXAFS enable the metal properties to be studied without significant interference from the support. In addition, catalysis studies often demand _in situ_ measurements, while the catalyst is treated by temperature cycling and/or exposure to gas environments. This is possible with EXAFS because the x-ray energies involved permit the use of reasonable window and sample cell structures. Such an apparatus has been described by Lytle et al.[26,29] In addition the speed of measurement, especially when synchrotron radiation is employed, is sufficient for a catalyst to be maintained in a stable state long enough for analysis.

The structural properties of the metal atoms depend greatly on the dispersion, or fraction of metal atoms exposed at the surface of a catalyst particle. Typically, supported metal catalysts having dispersions greater than ~0.5 correspond to particle sizes below ~20 Å and contain fewer than 100 atoms. Clearly such a configuration would be expected to depart from bulk structural and electronic properties, especially when there is interaction with the electronegative support and chemisorption of reactant and product molecules.

The contribution of EXAFS spectroscopy has been to make possible measurement of structural parameters including bond lengths, coordination numbers, disorder parameters and degree of bonding interaction to the support. In addition to the details available in the EXAFS spectrum, much can be deduced from analysis of the near-edge portion of the x-ray absorption spectrum,[29] especially the valence state of the catalyst metal atoms. While beyond the scope of this discussion, it is notable that the near edge structure that is measured simultaneously with the EXAFS carries information of comparable importance.

Several EXAFS studies of Pt, Os, Ir, and Ru on both silica and alumina supports[30-32] illustrate typical procedures. Catalysts were reduced in situ in flowing H_2 at ~425°C, followed by cooling in H_2 to 100°K for measurement of the x-ray absorption spectrum. Measurement was made by the absorption technique, which provided sufficient sensitivity for the 1 wt. % or greater metal loadings studied. Analysis procedures have been described extensively elsewhere;[26,31,33] they employed the single scattering EXAFS equation with the assumption of small disorder (see below). A nonlinear least squares procedure fitted the model EXAFS function to the Fourier filtered and k^3 weighted data. Reference functions for the backscattering amplitude and the phase function were deduced from measured EXAFS spectra for appropriate metal or solid compound reference materials. Results showed the reduction in nearest neighbor coordination number that would be expected for highly dispersed material, typically about 60% of the bulk value. Trends in the coordination numbers with different catalysts at the same loading suggest important limitations in the use of chemisorption isotherms in determining dispersion in catalysts.[31] Nearest neighbor bond lengths were found to agree with those of bulk metals within an uncertainty of 0.01 Å, but a tendency to show smaller

bond lengths is suggested. Finally, the disorder measured for these materials at 100°K exceeded that of the bulk metals by a factor of 1.4-2. To these quantitative factors can be added valuable qualitative information such as the changes observed in the appearance of the Fourier transforms of the EXAFS spectra due to oxidation and reduction cycles and temperature processing. An example is given in Fig. 1, in which reduced, O_2-chemisorbed and oxidized states of a Ru catalyst are compared to Ru metal and RuO_2. Numerous other EXAFS studies of this type have been reported.[34-38] These examples include metal-oxide catalysts, multi-component systems, as well as alloy catalysts.

One important application of the structural data derived from these studies is to estimate the type of structures represented by the small metal clusters. One approach has been that of Greegor and Lytle,[39] who measured coordination numbers for first, second, and third nearest neighbors in several catalyst metals. Ratios of these values to the corresponding coordination numbers for the same metals in bulk were then compared to values expected from models corresponding to particle sizes deduced from chemisorption measurements of dispersion. Models were made for various shapes, e.g. spheres, cubes, or disks. Results favored disk-like structures for Os, spheres for Cu, Ru, and Ir, and mixed shapes for Pt.

EXAFS derived results for small Pt particles caged in zeolite[40,41] have been compared with the extensive literature[42] describing the stability and structure of small particles. The Pt particles had mean sizes of ~12 Å. Particles analyzed under vacuum exhibited a strong contribution (~1/3) due to a form having reduced bond length, as would be expected for icosahedral particles. This result would be in accord with the expected stabilization of small clusters having 155 atoms into icosahedra.

Marques and Sandstrom are currently studying the temperature dependence of the structure of supported Pt catalysts, and observe a temperature dependent

bond length reduction for highly dispersed (~0.9) samples.[43] These particles
are expected to have average dimensions <10 Å. Average disorder is found to
be 1.5 to 2 times the bulk disorder, and exhibits the same temperature depen-
dence as the bulk. It is thought that the temperature dependent contraction
is an effect of the added disorder, possibly associated with the presence of
icosahedral and fcc particles. This is suggested by the behavior of the phase
of the EXAFS oscillations, which show a systematically increasing phase lag at
higher k-values, increasing with temperature. This is similar to the disorder
effects described in Zn by Eisenberger and Brown.[5] Modeling of the effective
pair distribution functions expected for such systems is being carried out.
Clearly, these systems are examples of high disorder, where the low-disorder
EXAFS equation must be applied with care.

DATA ANALYSIS

The following discussion will describe techniques in common use for
treatment of EXAFS data and determination of structural parameters. Both
pretreatment, that is extraction of the EXAFS spectrum from the raw x-ray
absorption data, and analysis of the EXAFS spectrum will be discussed. Emphasis
will be placed on the practical implementation of these analysis methods on a
small minicomputer system. For example, all of the procedures to be described
are carried out by the author on a 16-bit minicomputer (Digital Equipment
Corp. LSI-11/23) having 256 kilobytes of main memory and 1 megabyte of flexible
disk storage. Graphic display of data is via a direct view storage tube
graphic terminal (Tektronics Inc.).

Spectrum Acquisition

A discussion of experimental techniques for EXAFS is beyond the scope
of this article, but data analysis considerations obviously enter in planning

for data acquisition. Most EXAFS spectra are measured by sequentially measure-ing the x-ray absorption at a series of predetermined settings of a crystal monochromator. Ordinarily, a computer sets the monochromator via a stepping motor drive and also operates detectors, stores the data and performs other essential functions on-line to the experiment. Control programs in common use (e.g. that of Kirby[44]) provide for scanning over a predetermined range in step number or Bragg angle Θ, and for subdivision of this range into several subranges for which the spacing of the individual data points can be indepen-dently set.

The problem, then, is to decide on the size of the overall scan region, the positions of the breakpoints between the subregions, and the spacing of the data points in each subregion. Several considerations apply. In the x-ray energy range below the absorption edge several hundred eV are ordinarily scan-ned to determine the trend of the background absorption. Here resolution is not important so that the Bragg angle intervals between data points can corre-spond to fairly large energy intervals (e.g. 25 eV). In the region immediately below and above the absorption edge, near-edge structure may be important. In any case a careful determination of the edge position is needed for calibration purposes, indicating a fine scan over this region. Here, within ~25-40 eV of the absorption edge, the data points may have spacings as close as 1 eV or less, depending on the resolution of the spectrometer. The EXAFS region starts just above the absorption edge and extends to 1000-1500 eV above the edge, depending on how rapidly the oscillations damp out, and whether other features limit the scan. For example, an L_{III} edge scan is usually limited by the position of the L_{II} edge. The full range of the EXAFS region scan can be subdivided into three or more subregions.

Planning of these regions should be based on the ultimate objective of displaying the data in k (wave vector) space, where $k = \sqrt{2m(\hbar\omega - E_K)}/\hbar$. To facilitate accurate interpolation of the data onto an equally spaced k-grid, planning should reduce the variation in k-spacing between data points to the greatest extent possible. A useful strategy is to choose the limits of the subregions of the EXAFS region to provide for the same fractional change in k in each subregion. This is accomplished by letting

$$\frac{k_{i+1}}{k_i} = \left(\frac{k_{max}}{k_{min}}\right)^{1/n},$$

where k_i is the starting point and k_{i+1} the end point of the ith subregion, k_{min} and k_{max} are the starting and ending points of the whole EXAFS region, and n is the number of subregions. During a scan, the fact that the data points are spaced at fixed θ intervals $\Delta\theta$ means that the k-spacing between data points varies across each subregion according to $\Delta k = (dk/d\theta)\Delta\theta$. This effect can be minimized by choosing the median Δk value

$$\Delta k_m = \frac{1}{2}\left| \left(\frac{dk}{d\theta}\right)_{\theta_i} + \left(\frac{dk}{d\theta}\right)_{\theta_{i+1}} \right| \Delta\theta$$

the same in each subregion. A value of 0.05 $\overset{\circ}{A}^{-1}$ gives a suitable number of data points. The above considerations could be eliminated by writing a control program that scans at approximately equal k-intervals in the EXAFS region. To date the advantage of this approach has not been sufficient to motivate its implementation, for example, at the SSRL facility.

Background Subtraction

Following calculation of the x-ray photon energy values for the data points from Bragg's formula, the next step of data anlysis is to carefully calibrate the spectrum by setting the origin of the photoelectron energy scale at the position of the absorption edge of a suitable pure reference substance

(e.g. a metal foil) for which a spectrum was measured concurrently with the material being analyzed.

Subsequently, the smooth background can be subtracted to isolate the EXAFS oscillations. This operation is better carried out in E-space (E = photoelectron energy) than in k-space, because of excessive curvature that appears at low k-values in a k-space display. Some care must be taken in choosing the end points of the EXAFS region for this operation, especially the low end, to avoid influencing the smooth background by including non-EXAFS sharp features near the absorption edge. A cubic smoothing spline algorithm works very well for approximating the smooth background.[27,45] The spline can be calculated over equal or varying size subregions to control its "stiffness" to suit the shape of the background. Usually three equal subregions are satis-factory. The smoothing must of course be carried out on data points having equally spaced E-values, requiring interpolation. Cubic interpolation splines[45] which are fast and accurate, are very satisfactory for this purpose. At this stage, the interpolation need only be carried out for calculation of the smooth background. Subtraction of the smooth background can be made at the E-values of the original data points, so that the approximately uniform k-spacing is retained and the effect of the interpolation is not propagated forward.

An example of smooth background subtraction is given in Fig. 2. Note that the height of the absorption edge jump is determined at this stage by extrapolation of the smooth background, and used to normalize the EXAFS ampli-tude.

The data are now ready to be replotted in k-space. The parameter E_0 (the background potential) could be introduced at this point as a correction to the scale of E. It seems preferable to leave this to a separate analysis step, and determine k from $k = \sqrt{2mE}/\hbar$. An example of the resulting EXAFS

spectrum, corresponding to the absorption spectrum given in Fig. 2 is shown
in Fig. 3.

Fourier Transform

The Fast Fourier Transform (FFT) algorithm for discrete Fourier trans-
form is efficient and easily programmed.[46] It can be applied directly to the
k-space spectrum, in which case the input to the FFT is a real vector, or the
EXAFS spectrum can first be multiplied by $\exp[-i\phi(k)]$ to remove the effect of
a known phase function $\phi(k)$, as will be discussed later. In the latter case,
the input to the FFT is a complex vector and requires twice the storage area
in computer memory. The size of the FFT determines the resolution in transform
space, (r-space) because the spacing between adjacent r-space harmonics, Δr,
is related to the full k-range represented by the input vector to the FFT by
$\Delta r = \pi/k_f$, where the full input k-range runs from zero to k_f. (To preserve
the phase information in the EXAFS spectrum, the FFT input vector should
start with $k = 0$; zeros can pad the vector out to the start of the data.) To
achieve reasonable resolution in r-space, the input k-range must be made con-
siderably larger than the range of the EXAFS spectrum by padding the input
vector with zeros from the end of the data to k_f. The size of the transform
chosen and k_f will fix the required resolution of the data in k-space according
to $\Delta k = k_f/N$, where Δk is the size of the required k-space grid, and N is
the transform size (usually a power of 2). For example, a 4096 point transform
of data padded out to 96 Å^{-1} will require interpolation of the data on a k-space
grid at intervals of 0.0234 Å^{-1}. The resulting Fourier transform will have an
r-space grid interval of 0.0327 Å.

Before transforming, the k-space data are often multiplied by powers
of k to provide a more uniform weighting across the spectrum. In addition,

the portions of the data to be transformed are usually selected by a window function to take the amplitude smoothly to zero at the end points. This is for the purpose of reducing termination ripples, or leakage of the corresponding harmonics to adjacent portions of the spectrum in r-space.[46] Various windows are used in digital signal processing, including Hanning, Gaussian, and modifications that only effect a few percent at the ends of the k-range. These have been discussed extensively.[27,46,47]

Figure 4 shows the Fourier transform of the Pt data of Figs. 2 and 3, taken without any correction for the effect of the phase function $\phi(k)$.

Care must be taken not to interpret the Fourier Transform as a radial distribution function, because of nonlinear interplay between the disorder parameter σ and both the height and width of the Fourier transform peak. A study of this effect has been reported by Greegor and Lytle[48] for the case of Cu by comparing data taken over a wide range of temperatures for which the disorder was accurately known.

Inverse Transform

To isolate the EXAFS contribution due to a single feature in the Fourier transform, the inverse transform of the corresponding portion of the r-space spectrum can be taken. In doing this, it must be remembered that the r-space harmonics contained in the lower half of the transform also appear folded into the upper half by the phenomenon known as aliasing.[46] The entire upper half transform, or "fold," must be set to zero along with the harmonics outside the selected feature in the lower half. Both the real and imaginary parts of the complex transform are set to zero outside the selected range. A rectangular window function can be used to select the desired feature if the cutoff points correspond to harmonics of small magnitude, but smooth window

functions are sometimes used. The resulting complex vector is then used as input to the inverse FFT, resulting in a complex vector in k-space. The real part of this result represents the isolated EXAFS function corresponding to the feature selected in r-space. The overall phase $\Phi(k)$ of this EXAFS function is given by adding $\pi/2$ to the argument of the complex k-space vector. The $\pi/2$ term is associated with setting the "fold" components to zero in r-space.[27] An inverse transform (real part) of the major feature of the Fig. 4 Fourier transform is shown in Fig. 5.

Phase Functions

The total phase of the Fourier filtered EXAFS spectrum corresponds to $\Phi(k) = 2kr + \phi(k)$, where r is the bond length giving rise to the selected Fourier transform feature. If r is known, as for a reference substance, then $\phi(k)$ can be calculated directly. The only ambiguity is the effect of E_0, which determines the k scale according to $k = \sqrt{2m(E-E_0)}/\hbar$. A change in the E_0 value by ΔE_0 modifies the phase function[49,50] according to

$$\phi'(k') \simeq \phi(k) + 2mr\Delta E_0/k\hbar^2$$

where

$$k' = (k^2 - 2m\Delta E_0/\hbar^2)^{1/2} .$$

In the case of a reference substance for which r is known, it may be desirable to find the E_0 value that gives the best agreement between the empirically determined phase functions and theoretical phase functions.[50] Alternatively, if a theoretical or empirical reference phase function is available, both E_0 and r can be adjusted in calculating $\phi(k)$ from $\Phi(k)$ to fit the phase of the unknown substance to that of the standard.

This is the phase fitting technique referred to earlier.[9] It is equivalent to the "constant r" method described by Martens et al.,[47] for which E_0 is adjusted to give a constant value of

$$r(k) = [\Phi(k) - \phi(k)]/2k$$

over the widest k-range, with the resulting constant value to be assigned to the bond length.

Figure 6 shows $\phi(k)$ for the Pt metal first neighbor bond in comparison with the theoretical calculation of Teo and Lee.[50] Here r was fixed at the crystallographic value at 100°K of 2.769 Å, and E_0 was adjusted for best fit, giving a value of 5.35 eV.

Fourier Transform Modified by Phase Function

When the phase function $\phi(k)$ is known empirically as described above, or is available from theory, it is an advantage in some situations to calculate a modified Fourier transform of the EXAFS spectrum by first multiplying the data by $\exp[-i\phi(k)]$. Transforming the resulting complex vector is then equivalent to transforming the data with respect to the full phase argument.[49,51] This type of transform has the advantage of providing a criterion for selecting E_0, as shown by Lee and Beni.[49] When E_0 is adjusted so that $\phi(k)$ is accurate for the given spectrum, the imaginary part and magnitude of the transform should align at the correct bond distance. Note that this procedure is only useful when the EXAFS oscillations are all due to the same absorber-scatterer pair (or at least when features in the Fourier transform due to different absorber-scatterer pairs are well separated), since only one phase function can be removed at a time.

Figure 7 shows the phase removed transform of the Pt data of Fig. 3, for which the theoretical phase function shown in Fig. 6 was used. In Fig. 7 each coordination distance is represented by a single peak with minor side lobes (due to the k-dependence of the amplitude function and the windowing used). In contrast, the complicated behavior of $\phi(k)$ for Pt-Pt causes the normal Fourier transform (Fig. 5) to have extremely complicated structure. The phase removed transform has proved to be useful in studies of Pt catalysts, because it greatly aids in the isolation of the first neighbor peak from the second neighbor and the Pt-O coordinations due to the support. Subsequent inverse transforms are ready for analysis by curve fitting without use of $\phi(k)$, because the phase of the resulting inverse transform represents only any differences between the material being studied and the reference. This residual is significant in the analysis of disorder effects as discussed in the example of Pt catalysts.[43]

Curve Fitting

The real part of the inverse transform is the input for the model function curve fitting techniques that are widely used to extract bond distances, coordination numbers and disorder parameters. The model function for k-space analysis has usually been the familiar EXAFS equation that applies in the limit of small disorder:

$$\chi(k) = \sum_j A_j(k)\sin[2kr_j + \phi_j(k)] .$$

Here the sum extends over all the coordination shells (radii r_j) included in the inverse transform and $\phi_j(k)$ is the phase function for the jth shell. The amplitude $A_j(k)$ is

$$A_j(k) = (N_j/kr_j)|f_j(k,\pi)|\exp(-2k^2\sigma^2) ,$$

where N_j, f_j, and σ_j are, respectively, the coordination number, backscattering amplitude and disorder parameter for the jth shell.

Curve fitting procedures for the EXAFS equation have been reviewed in detail,[27,33] and also discussed in the specific applications of solutions[14] and catalysts.[26]

Other Techniques

The above summarizes analysis procedures that have been widely applied, especially to solutions and catalysts. Many variations and alternative methods are in common use, especially for disordered systems. Examples include analysis of beats in the EXAFS oscillations to resolve near bond distances,[52] fitting of model functions to the r-space transform of the data,[53] and various analyses of the phase and amplitude effects of disorder.[5,43,51,54,55]

ACKNOWLEDGMENTS

REFERENCES

[1] See, for example: <u>Water, a Comprehensive Treatise</u>, edited by F. Franks (Plenum, New York, 1973), Vol. 3.

[2] H. S. Frank and W. Y. Wen, Discuss. Faraday Soc. <u>24</u>, 133 (1957).

[3] G. W. Neilson and J. E. Enderby in <u>Annual Reports on the Progress of Chemistry</u>, edited by M. C. R. Symons, 76C, 185 (1979).

[4] P. Eisenberger and B. M. Kincaid, Chem. Phys. Lett. <u>36</u>, 134 (1975).

[5] P. Eisenberger and G. S. Brown, Solid State Comm. <u>29</u>, 481 (1979).

[6] H. Winick and A. Bienenstock, Ann. Rev. Nucl. Part. Sci. <u>28</u>, 33 (1973).

[7] J. B. Hastings, in <u>EXAFS Spectroscopy</u>, edited by B. K. Teo and D. C. Joy (Plenum, New York, 1981), p. 171.

[8] D. R. Sandstrom, H. W. Dodgen, and F. W. Lytle, J. Chem. Phys. <u>67</u>, 473 (1977).

[9] D. R. Sandstrom, B. R. Stults, and R. B. Greegor, in <u>EXAFS Spectroscopy</u>, edited by B. K. Teo and D. C. Joy (Plenum, New York, 1981), p. 139.

[10] R. Caminite, G. Licheri, G. Piccaluga, and G. Pinna, Faraday Discuss. Chem. Soc. <u>64</u>, 62 (1978).

[11] M. Magini, J. Chem. Phys. <u>74</u>, 2523 (1981).

[12] R. Caminiti, G. Licheri, G. Paschina, G. Piccaluga, and G. Pinna, Z. Naturforsch. <u>35a</u>, 1361 (1980).

[13] A. K. Soper, G. W. Neilson, J. E. Enderby, and R. A. Howe, J. Phys. C <u>10</u>, 1793 (1977); G. W. Neilson and J. E. Enderby, J. Phys. C <u>11</u>, L625 (1978).

[14] D. R. Sandstrom, J. Chem. Phys. <u>71</u>, 2381 (1979).

[15] P. Lagarde, A. Fontaine, D. Raoux, A. Sadoc, and P. Migliardo, J. Chem. Phys. <u>72</u>, 3061 (1980).

[16] M. P. Fontana, G. Maisano, P. Migliardo, and F. Wanderlingh, J. Chem. Phys. <u>69</u>, 676 (1978).

[17]J. R. Bell, J. L. Tyvoll, and D. L. Wertz, J. Am. Chem. Soc. 95, 1456 (1973); D. L. Wertz and J. L. Tyvoll, J. Inorg. Nucl. Chem. 36, 3713 (1974).

[18]A. Fontaine, P. Lagarde, D. Raoux, M. P. Fontana, G. Maisano, P. Migliardo, and F. Wanderlingh, Phys. Rev. Lett. 41, 504 (1978).

[19]J. M. Fine, Ph.D. Thesis, Washington State University, 1981.

[20]A. Sadoc, A. Fontaine, P. Lagarde, and D. Raoux, J. Am. Chem. Soc. 103, 6287 (1981).

[21]T. M. Hayes and J. B. Boyce, in EXAFS Spectroscopy, edited by B. K. Teo and D. C. Joy (Plenum, New York, 1981), p. 81.

[22]S. P. Cramer and K. O. Hodgson, in Progress in Inorganic Chemistry, edited by S. J. Lippard (Wiley, New York, 1979), Vol. 25, p. 1.

[23]B. R. Stults, R. M. Friedman, K. Koenig, W. Knowles, R. B. Greegor, and F. W. Lytle, J. Am. Chem. Soc. 103, 3235 (1981).

[24]J. Reed, P. Eisenberger, B. K. Teo, and B. M. Kincaid, J. Am. Chem. Soc. 99, 5217 (1977); J. Am. Chem. Soc. 100, 2375 (1978).

[25]T. E. Madey, J. T. Yates, Jr., D. R. Sandstrom, and R. J. H. Voorhoeve, in Treatise on Solid State Chemistry, edited by N. B. Hannay (Plenum, New York, 1976), Vol. 6B, pp. 1-124.

[26]F. W. Lytle, G. H. Via, and J. H. Sinfelt in Synchrotron Radiation Research, edited by H. Winick and S. Doniach (Plenum, New York, 1980), p. 401.

[27]P. A. Lee, P. H. Citrin, P. Eisenberger, and B. M. Kincaid, Rev. Mod. Phys. 53, 769 (1981).

[28]J. H. Sinfelt, Rev. Mod. Phys. 51, 569 (1979).

[29]F. W. Lytle, P. S. P. Wei, R. B. Greegor, G. H. Via, and J. H. Sinfelt, J. Chem. Phys. 70, 4849 (1979).

[30] F. W. Lytle, G. H. Vìa, and J. H. Sinfelt, J. Chem. Phys. 67, 3831 (1977).

[31] J. H. Sinfelt, G. H. Via, and F. W. Lytle, J. Chem. Phys. 68, 2009 (1978).

[32] G. H. Via, J. H. Sinfelt, and F. W. Lytle, J. Chem. Phys. 71, 690 (1979).

[33] D. R. Sandstrom and F. W. Lytle, Ann. Rev. Phys. Chem. 30, 215 (1979).

[34] I. W. Bassi, F. W. Lytle, and G. Parravano, J. Catalysis 42, 139 (1976).

[35] R. M. Friedman, J. J. Freeman, and F. W. Lytle, J. Catalysis 55, 10 (1978).

[36] J. H. Sinfelt, G. H. Via, and F. W. Lytle, J. Chem. Phys. 72, 4832 (1980).

[37] D. R. Short, M. R. Kelly, J. R. Katzer, and S. Khalid, J. Catalysis, in press.

[38] R. B. Greegor, F. W. Lytle, R. L. Chin, and D. M. Hercules, J. Phys. Chem. 85, 1232 (1981).

[39] R. B. Greegor and F. W. Lytle, J. Catalysis 63, 476 (1980).

[40] B. Moraweck, G. Clugnet, and A. J. Renouprez, Surface Science 81, L631 (1979).

[41] B. Moraweck and A. J. Renouprez, Surface Science 106, 35 (1981).

[42] M. R. Hoare, Adv. Chem. Phys. 40, 49 (1979).

[43] E. C. Marques and D. R. Sandstrom, to be published.

[44] J. A. Kirby, "Manual for Data Collection Program," Report No. UCID-4017, Lawrence Berkeley Laboratory, Berkeley, California 94720, Feb. 1978.

[45] C. de Boor, A Practical Guide to Splines (Springer-Verlag, New York, 1978).

[46]See, for example, C. K. Yuen, _Digital Spectral Analysis_ (Fearon Pitman, 1979), or P. Bloomfield, _Fourier Analysis of Time Series_ (Wiley, New York, 1976).

[47]G. Martens, P. Rabe, N. Schwentner, and A. Werner, Phys. Rev. B $\underline{17}$, 1481 (1978).

[48]R. B. Greegor and F. W. Lytle, Phys. Rev. B $\underline{20}$, 4902 (1979).

[49]P. A. Lee and G. Beni, Phys. Rev. B $\underline{15}$, 2862 (1977).

[50]B. K. Teo and P. A. Lee, J. Am. Chem. Soc. $\underline{101}$, 2815 (1979).

[51]E. D. Crozier and A. J. Seary, Can. J. Phys. $\underline{58}$, 1388 (1980).

[52]G. Martens, P. Rabe, N. Schwentner, and A. Werner, Phys. Rev. Lett. $\underline{22}$, 1411 (1977).

[53]T. M. Hayes, J. Non. Cryst. Solids $\underline{31}$, 57 (1978).

[54]J. J. Rehr, Phys. Rev. B, in press.

[55]G. Bunker (private communication).

TABLE I

Solute	Concentration (Moles/liter)	Coordination	Bond Length (Angstroms)	Reference
$CuBr_2$		Cu–O	1.97 ± 0.08	4
		Br–O	3.14 ± 0.1	4
$Ni(NO_3)_2 \cdot 6(H_2O)$	0.1 M	Ni–O	2.05	8
$Ni(NO_3)_2 \cdot 6(H_2O)$	0.1 M	Ni–O	2.06 ± 0.01	9
$Co(NO_3)_2 \cdot 6(H_2O)$	0.1 M	Co–O	2.08 ± 0.01	9
$Cr(NO_3)_3 \cdot 6(H_2O)$	0.1 M	Cr–O	2.01 ± 0.01	9

TABLE II

Solute	Concentration	Method	Principal Results	Reference
$NiCl_2$	4 M and 2 M	XRD	Ni^{2+} ions fully hydrated. $Ni-H_2O$ distance: 4 M, 2.062 Å; 2 M, 2.069 Å.	10
$NiCl_2$	2.95 M	XRD	Ni^{2+} ions fully hydrated, or up to 50% contribution of $Ni(H_2O)_5Cl^+$.	11
$NiCl_2$	1.96 and 3.88 M	XRD	Ni^{2+} ions fully hydrated, but evidence presented for sharing of water molecules by neighboring anion and cation coordination shells. $Ni-H_2O$ distances: 1.96 M, 2.063 Å; 3.88 M, 2.068 Å.	12
$NiCl_2$	0.086 - 4.41 M (In D_2O)	ND	Ni^{2+} ions fully hydrated. At highest concentrations $Ni-O$ distance is 2.07 Å. Angle between D_2O plane and $Ni-D$ axis ~45° at highest concentrations, decreasing to zero at lowest concentration.	13
$NiCl_2$	2.78 and 3.74 M	EXAFS	Ni^{2+} ions fully hydrated. $Ni-O$ distances: 2.78 M, 2.06 Å; 3.74 M, 2.07 Å. Evidence for Cl^- in second coordination sphere of Ni^{2+}.	14
$NiCl_2$	0.5 and 4.0 M	EXAFS	Very little or no $Ni-Cl$ bonding.	15
$NiCl_2$	0.21 - 4.2 M	Raman	At highest concentrations, ~50% of Ni^{2+} in $NiCl_4^{2-}$ complexes.	16

TABLE II (continued)

Solute	Concentration	Method	Principal Results	Reference
$NiBr_2$	0.4 and 4.0 M	EXAFS	Little or no Ni–Br bonding.	15
$CuCl_2$	2.95 M	XRD	Cu^{2+} coordinated by average of 1.2 equatorial Cl^- ions, 2.8 equatorial water molecules, and identity of axial coordination ambiguous.	11
$CuCl_2$	3.3 and 4.4 M*	XRD	3.3–3.6 Cl^- ions in primary coordination sphere of Cu^{2+}.	17
$CuCl_2$	0.05 and 4.86 M	EXAFS	Cu–Cl bonding evident at high concentration.	15
$CuBr_2$	0.05 – 4.5 M	EXAFS	50% of Cu^{2+} ions bound in linked planer $CuBr_4$ structure as in crystal.	15,18
$CuBr_2$	3.3 and 4.4 M*	EXAFS	Multiple mononuclear $CuBr_n(H_2O)_{n-6}^{2-n}$ complexes.	19
$ZnBr_2$	8.08 M	EXAFS	Zn^{2+} in linked $ZnBr_4$ tetrahedra similar to crystal.	15
$ZnBr_2$	0.05 – 5.3 M (in ethyl acetate)	EXAFS	Zn^{2+} in linked $ZnBr_4$ tetrahedra similar to crystal.	20

*Concentrations shown for stoichiometric solutions. Study also investigated non-stoichiometric solutions.

Figure 4. Magnitude of the Fourier transform of the Pt metal EXAFS oscil-
lations shown in Fig. 3 after weighting by k. Radius scale in Å.
Data in the range 4.4 – 14.3 $\overset{\circ}{A}{}^{-1}$ have been selected for transform
by a half-cosine bell window function applied to 10% of the above
range at both ends of the range. The 4096 points transformed
correspond to a full k-range of 96 $\overset{\circ}{A}{}^{-1}$.

Figure 5. Inverse Fourier transform (real part) of the complex transform
for which the magnitude is shown in Fig. 4, after setting to zero
all harmonics outside the vertical bars on Fig. 4. The result
corresponds to the first shell contribution in Pt metal at 100°K.
The effect of weighting by k and windowing have not been removed
from the inverse transform. Wave vector scale (k-scale) same as
Fig. 3.

Figure 6. Comparison of empirical and theoretical phase function for Pt metal
at 100°K. Solid curve: Phase of the inverse transform oscillations
shown in Fig. 5 determined as described in text, minus 2kr for
r = 2.769 Å. Dotted curve: Theoretical calculation for Pt absor-
ber (ℓ=2) and Pt scatterer.[50] Multiples of 2π have been used to
shift the curves into alignment. E_0 has been adjusted for the
empirical phase function to give best agreement, resulting in
E_0 = 5.35 eV. Wave vector scale (k-scale) same as Fig. 3.

Figure 7. Magnitude (envelope curve) and imaginary part of phase removed
Fourier transform of Pt metal EXAFS oscillations shown in Fig. 3,
using theoretical phase function shown in Fig. 6, and E_0 shift of
5.35 eV. Radius scale same as Fig. 4.

CAPTIONS FOR FIGURES

Figure 1. EXAFS spectra (a,b,c,d, and e) and corresponding Fourier transforms
           (A,B,C,D, and F) for Ru: (a,A) 1% Ru on SiO_2 catalyst, reduced in
           H_2; (b,B) after exposure to 1011 pa O_2 at 25°C; (c,C) after exposure
           to O_2 at 400°C; (d,d) Ru metal; (e,E) RuO_2. From Ref. 26.

Figure 2. X-ray absorption spectrum measured at the $Pt-L_{III}$ edge, for Pt
           metal (2.5 µm foil) at 100°K. Energy scale relative to edge energy
           of 11563.7 eV. Absorption scale given by $\ln(I_0/I)$, where I_0 and I
           represent the incident and transmitted beam detector signals
           respectively. The smooth curve drawn through the data was gener-
           ated by a cubic smoothing spline calculated on three equally spaced
           regions delimitated by the two crosses drawn on the data. The
           spacing of the two crosses to the left of the edge gives an esti-
           mate of the absorption edge jump obtained by extrapolation of the
           spline curve to a point (upper cross) directly above the pre-edge
           absorption minimum (lower cross).

Figure 3. EXAFS oscillations vs photoelectron wave vector k $\overset{\circ}{A}^{-1}$, for Pt
           metal data shown in Fig. 2. The ordinate chi is given by the
           difference of the x-ray absorption and the spline curve shown in
           Fig. 2, divided by the absorption edge jump. The wave vector
           scale has been calculated from k = $\sqrt{0.263E}$, where E is the energy
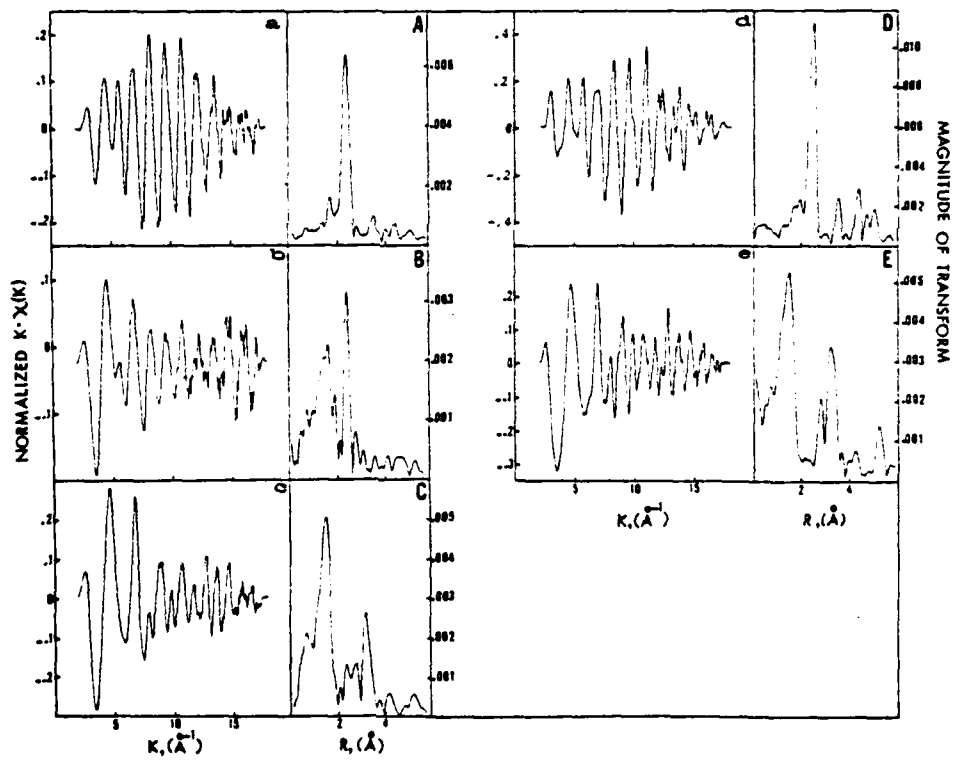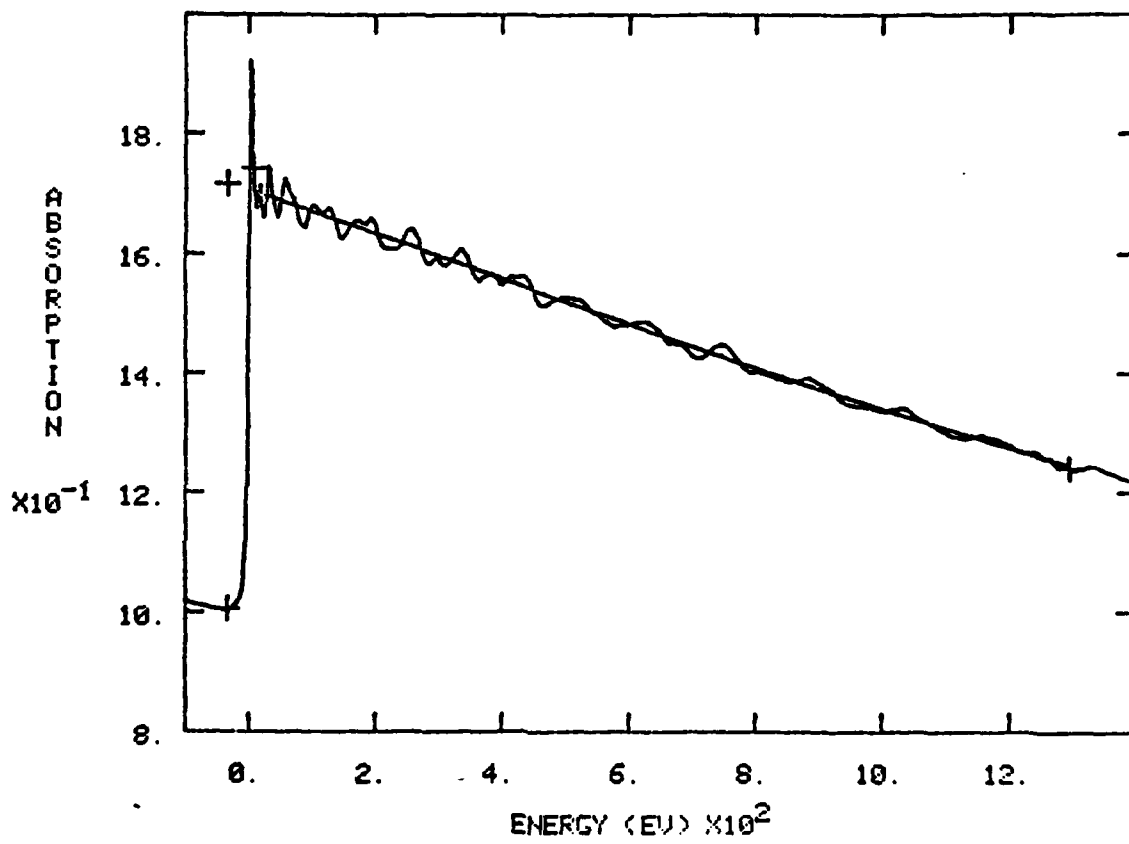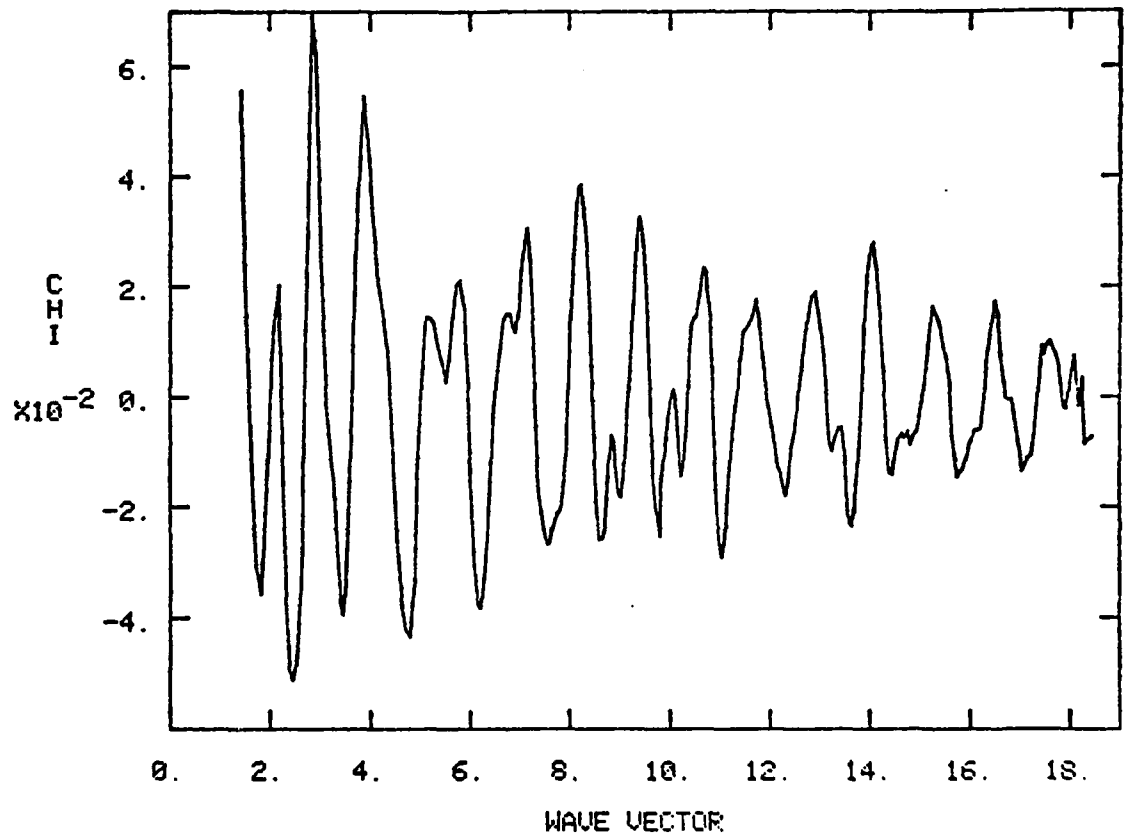   scale in Fig. 2.

NORMALIZED K·X(K)

MAGNITUDE OF TRANSFORM

K,(Å⁻¹)   R,(Å)

Fig. 1

ABSORPTION

X10^{-1}

18.

16.

14.

12.

10.

8.
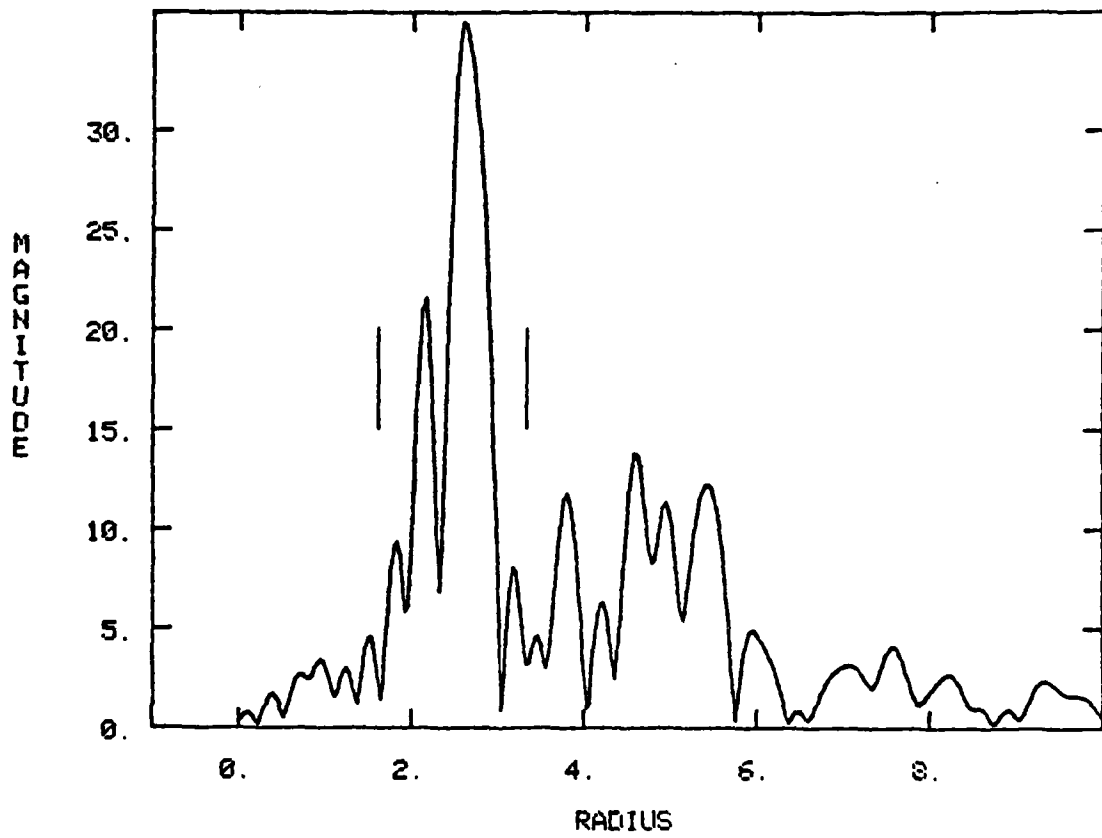
0.   2.   4.   6.   8.   10.   12.

ENERGY (EV) X10^{2}

Fig 2

Fig 4

Fig. 7

TECHNICAL REPORT DISTRIBUTION LIST, GEN

	No. Copies		No. Copies
Office of Naval Research Attn: Code 413 800 N. Quincy Street Arlington, Virginia 22217	2	Naval Ocean Systems Center Attn: Technical Library San Diego, California 92152	1
ONR Pasadena Detachment Attn: Dr. R. J. Marcus 1030 East Green Street Pasadena, California 91106	1	Naval Weapons Center Attn: Dr. A. B. Amster Chemistry Division China Lake, California 93555	1
Commander, Naval Air Systems Command Attn: Code 310C (H. Rosenwasser) Washington, D.C. 20360	1	Scientific Advisor Commandant of the Marine Corps Code RD-1 Washington, D.C. 20380	1
Naval Civil Engineering Laboratory Attn: Dr. R. W. Drisko Port Hueneme, California 93401	1	Dean William Tolles Naval Postgraduate School Monterey, California 93940	1
Superintendent Chemistry Division, Code 6100 Naval Research Laboratory Washington, D.C. 20375	1	U.S. Army Research Office Attn: CRD-AA-IP P.O. Box 12211 Research Triangle Park, NC 27709	1
Defense Technical Information Center Building 5, Cameron Station Alexandria, Virginia 22314	12	Mr. Vincent Schaper DTNSRDC Code 2830 Annapolis, Maryland 21402	1
DTNSRDC Attn: Dr. G. Bosmajian Applied Chemistry Division Annapolis, Maryland 21401	1	Mr. John Boyle Materials Branch Naval Ship Engineering Center Philadelphia, Pennsylvania 19112	
Naval Ocean Systems Center Attn: Dr. S. Yamamoto Marine Sciences Division San Diego, California 91232	1	Mr. A. M. Anzalone Administrative Librarian PLASTEC/ARRADCOM Bldg 3401 Dover, New Jersey 07801	1

TECHNICAL REPORT DISTRIBUTION LIST, 359

Dr. Paul Delahay
Department of Chemistry
New York University
New York, New York 10003

Dr. P. J. Hendra
Department of Chemistry
University of Southampton
Southampton S09 5NH
United Kingdom

Dr. T. Katan
Lockheed Missiles and
  Space Co., Inc.
P.O. Box 504
Sunnyvale, California 94088

Dr. D. N. Bennion
Department of Chemical Engineering
Brighma Young University
Provo, Utah 84602

Dr. R. A. Marcus
Department of Chemistry
California Institute of Technology
Pasadena, California 91125

Mr. Joseph McCartney
Code 7121
Naval Ocean Systems Center
San Diego, California 92152

Dr. J. J. Auborn
Bell Laboratories
Murray Hill, New Jersey 07974

Dr. Joseph Singer, Code 302-1
NASA-Lewis
21000 Brookpark Road
Cleveland, Ohio 44135

Dr. P. P. Schmidt
Department of Chemistry
Oakland University
Rochester, Michigan 48063

Dr. H. Richtol
Chemistry Department
Rensselaer Polytechnic Institute
Troy, New York 12181

Dr. E. Yeager
Department of Chemistry
Case Western Reserve University
Cleveland, Ohio 44106

Dr. C. E. Mueller
The Electrochemistry Branch
Naval Surface Weapons Center
White Oak Laboratory
Silver Spring, Maryland 20910

Dr. Sam Perone
Chemistry & Materials
  Science Department
Lawrence Livermore National Lab.
Livermore, California 94550

Dr. Royce W. Murray
Department of Chemistry
University of North Carolina
Chapel Hill, North Carolina 27514

Dr. G. Goodman
Johnson Controls
5757 North Green Bay Avenue
Milwaukee, Wisconsin 53201

Dr. B. Brummer
EIC Incorporated
111 Chapel Street
Newton, Massachusetts 02158

Dr. Adam Heller
Bell Laboratories
Murray Hill, New Jersey 07974

Electrochimica Corporation
Attn: Technical Library
2485 Charleston Road
Mountain View, California 94040

Library
Duracell, Inc.
Burlington, Massachusetts 01803

Dr. A. B. Ellis
Chemistry Department
University of Wisconsin
Madison, Wisconsin 53706

TECHNICAL REPORT DISTRIBUTION LIST, GEN

	No. Copies		No Copies
Office of Naval Research Attn: Code 413 800 N. Quincy Street Arlington, Virginia 22217	2	Naval Ocean Systems Center Attn: Technical Library San Diego, California 92152	1
ONR Pasadena Detachment Attn: Dr. R. J. Marcus 1030 East Green Street Pasadena, California 91106	1	Naval Weapons Center Attn: Dr. A. B. Amster Chemistry Division China Lake, California 93555	1
Commander, Naval Air Systems Command Attn: Code 310C (H. Rosenwasser) Washington, D.C. 20360	1	Scientific Advisor Commandant of the Marine Corps Code RD-1 Washington, D.C. 20380	1
Naval Civil Engineering Laboratory Attn: Dr. R. W. Drisko Port Hueneme, California 93401	1	Dean William Tolles Naval Postgraduate School Monterey, California 93940	1
Superintendent Chemistry Division, Code 6100 Naval Research Laboratory Washington, D.C. 20375	1	U.S. Army Research Office Attn: CRD-AA-IP P.O. Box 12211 Research Triangle Park, NC 27709	1
Defense Technical Information Center Building 5, Cameron Station Alexandria, Virginia 22314	12	Mr. Vincent Schaper DTNSRDC Code 2830 Annapolis, Maryland 21402	1
DTNSRDC Attn: Dr. G. Bosmajian Applied Chemistry Division Annapolis, Maryland 21401	1	Mr. John Boyle Materials Branch Naval Ship Engineering Center Philadelphia, Pennsylvania 19112	1
Naval Ocean Systems Center Attn: Dr. S. Yamamoto Marine Sciences Division San Diego, California 91232	1	Mr. A. M. Anzalone Administrative Librarian PLASTEC/ARRADCOM Bldg 3401 Dover, New Jersey 07801	1

TECHNICAL REPORT DISTRIBUTION LIST, 359

Dr. M. Wrighton
Chemistry Department
Massachusetts Institute
  of Technology
Cambridge, Massachusetts 02139

Dr. M. M. Nicholson
Electronics Research Center
Rockwell International
3370 Miraloma Avenue
Anaheim, California

Dr. B. Stanley Pons
Department of Chemistry
University of Utah
Salt Lake City, Utah 84112

Dr. Michael J. Weaver
Department of Chemistry
Purdue University
West Lafayette, Indiana 47907

Donald E. Mains
Naval Weapons Support Center
Electrochemical Power Sources Division
Crane, Indiana 47522

Dr. R. David Rauh
EIC Corporation
111 Chapel Street
Newton, Massachusetts 02158

S. Ruby
DOE (STOR)
M.S. 6B025 Forrestal Bldg.
Washington, D.C. 20595

Dr. Aaron Wold
Department of Chemistry
Brown University
Providence, Rhode Island 02192

Dr. A. J. Bard
Department of Chemistry
University of Texas
Austin, Texas 78712

Dr. Martin Fleischmann
Department of Chemistry
University of Southampton
Southampton SO9 5NH ENGLAND

Dr. Janet Osteryoung
Department of Chemistry
State University of New York
Buffalo, New York 14214

Dr. R. A. Osteryoung
Department of Chemistry
State University of New York
Buffalo, New York 14214

Dr. Donald W. Ernst
Naval Surface Weapons Center
Code R-33
White Oak Laboratory
Silver Spring, Maryland 20910

Dr. Denton Elliott
Air Force Office of Scientific
  Research
Bolling AFB
Washington, D.C. 20332

Mr. James R. Moden
Naval Underwater Systems Center
Code 3632
Newport, Rhode Island 02840

Dr. R. Nowak
Naval Research Laboratory
Code 6130
Washington, D.C. 20375

Dr. Bernard Spielvogel
U.S. Army Research Office
P.O. Box 12211
Research Triangle Park, NC 27709

Dr. D. F. Shriver
Department of Chemistry
Northwestern University
Evanston, Illinois 60201

Dr. William Ayers
ECD Inc.
P.O. Box 5357
North Branch, New Jersey 08876

Dr. Aaron Fletcher
Naval Weapons Center
Code 3852
China Lake, California 93555

TECHNICAL REPORT DISTRIBUTION LIST, 359

Dr. David Aikens
Chemistry Department
Rensselaer Polytechnic Institute
Troy, New York 12181

Dr. A. P. B. Lever
Chemistry Department
York University ·
Downsview, Ontario M3J1P3

Dr. Stanislaw Szpak
Naval Ocean Systems Center
Code 6343, Bayside
San Diego, California 95152

Dr. Gregory Farrington
Department of Materials Science
 and Engineering
University of Pennsylvania
Philadelphia, Pennsylvania 19104

M. L. Robertson
Manager, Electrochemical
  and Power Sources Division
Naval Weapons Support Center
Crane, Indiana 47522

Dr. T. Marks
Department of Chemistry
Northwestern University
Evanston, Illinois 60201

Dr. Micha Tomkiewicz
Department of Physics
Brooklyn College
Brooklyn, New York 11210

Dr. Lesser Blum
Department of Physics
University of Puerto Rico
Rio Piedras, Puerto Rico 00931

Dr. Joseph Gordon, II
IBM Corporation
K33/281
5600 Cottle Road
San Jose, California 95193

Dr. D. H. Whitmore
Department of Materials Science
Northwestern University
Evanston, Illinois 60201

Dr. Alan Bewick
Department of Chemistry
The University of Southampton
Southampton, SO9 5NH ENGLAND

Dr. E. Anderson
NAVSEA-56Z33 NC #4
2541 Jefferson Davis Highway
Arlington, Virginia 20362

Dr. Bruce Dunn
Department of Engineering &
  Applied Science
University of California
Los Angeles, California 90024

Dr. Elton Cairns
Energy & Environment Division
Lawrence Berkeley Laboratory
University of California
Berkeley, California 94720

Dr. D. Cipris
Allied Corporation
P.O. Box 3000R
Morristown, New Jersey 07960

Dr. M. Philpott
IBM Corporation
5600 Cottle Road
San Jose, California 95193

Dr. Donald Sandstrom
Department of Physics
Washington State University
Pullman, Washington 99164

Dr. Carl Kannewurf
Department of Electrical Engineering
  and Computer Science
Northwestern University
Evanston, Illinois 60201

TECHNICAL REPORT DISTRIBUTION LIST, 359

Dr. Robert Somoano
Jet Propulsion Laboratory
California Institute of Technology
Pasadena, California 91103

Dr. Johann A. Joebstl
USA Mobility Equipment R&D Command
DRDME-EC
Fort Belvoir, Virginia 22060

Dr. Judith H. Ambrus
NASA Headquarters
M.S. RTS-6
Washington, D.C. 20546

Dr. Albert R. Landgrebe
U.S. Department of Energy
M.S. 6B025 Forrestal Building
Washington, D.C. 20595

Dr. J. J. Brophy
Department of Physics
University of Utah
Salt Lake City, Utah 84112

Dr. Charles Martin
Department of Chemistry
Texas A&M University
College Station, Texas 77843

Dr. H. Tachikawa
Department of Chemistry
Jackson State University
Jackson, Mississippi 39217

Dr. Theodore Beck
Electrochemical Technology Corp.
3935 Leary Way N.W.
Seattle, Washington 98107

Dr. Farrell Lytle
Boeing Engineering and
  Construction Engineers
P.O. Box 3707
Seattle, Washington 98124

Dr. Robert Gotscholl
U.S. Department of Energy
MS G-226
Washington, D.C. 20545

Dr. Edward Fletcher
Department of Mechanical Engineering
University of Minnesota
Minneapolis, Minnesota 55455

Dr. John Fontanella
Department of Physics
U.S. Naval Academy
Annapolis, Maryland 21402

Dr. Martha Greenblatt
Department of Chemistry
Rutgers University
New Brunswick, New Jersey 08903

Dr. John Wasson
Syntheco, Inc.
Rte 6 - Industrial Pike Road
Gastonia, North Carolina 28052

Dr. Walter Roth
Department of Physics
State University of New York
Albany, New York 12222

Dr. Anthony Sammells
Eltron Research Inc.
710 E. Ogden Avenue #108
Naperville, Illinois 60540

Dr. W. M. Risen
Department of Chemistry
Brown University
Providence, Rhode Island 02192

Dr. C. A. Angell
Department of Chemistry
Purdue University
West Lafayette, Indiana 47907

Dr. Thomas Davis
Polymer Science and Standards
  Division
National Bureau of Standards
Washington, D.C. 20234